Earth Syst. Dynam. Discuss., 5, 1197–1219, 2014
www.earth-syst-dynam-discuss.net/5/1197/2014/
doi:10.5194/esdd-5-1197-2014

Earth System Dynamics Discussions
Open Access

Decomposing uncertainties in the future terrestrial carbon budget associated with emission scenario, climate projection, and ecosystem simulation using the ISI-MIP result

K. Nishina[1], A. Ito[1], P. Falloon[3], A. D. Friend[5], D. J. Beerling[6], P. Ciais[7], D. B. Clark[4], R. Kahana[3], E. Kato[1], W. Lucht[2], M. Lomas[6], R. Pavlick[8], S. Schaphoff[2], L. Warszawaski[2], and T. Yokohata[1]

[1]National Institute for Environmental Studies, 16-2, Onogawa, Tsukuba, Ibaraki, Japan
[2]Met Office Hadley Centre, FitzRoy Road, Exeter, Devon, EX1 3PB, UK
[3]Department of Geography, University of Cambridge, Downing Place, Cambridge CB2 3EN, UK
[4]Potsdam Institute for Climate Impact Research, Telegraphenberg A 31, 14473, Potsdam, Germany
[5]Centre for Ecology and Hydrology, Wallingford, OX10 8BB, UK
[6]Department of Animal and Plant Sciences, University of Sheffield, Sheffield S10 2TN, UK

[7]Laboratoire des Sciences du Climat et de l'Environment, Joint Unit of CEA-CNRS-UVSQ, Gif-sur-Yvette, France
[8]Max Planck Institute for Biogeochemistry, Hans-Knöll-Str. 10, 07745 Jena, Germany

Received: 16 September 2014 – Accepted: 30 September 2014 – Published: 10 October 2014

Correspondence to: K. Nishina (nishina.kazuya@nies.go.jp)

Published by Copernicus Publications on behalf of the European Geosciences Union.

Abstract

Changes to global net primary production (NPP), vegetation biomass carbon (VegC), and soil organic carbon (SOC) estimated by six global vegetation models (GVM) obtained from an Inter-Sectoral Impact Model Intercomparison Project study were examined. Simulation results were obtained using five global climate models (GCM) forced with four representative concentration pathway (RCP) scenarios. To clarify which component (emission scenarios, climate projections, or global vegetation models) contributes the most to uncertainties in projected global terrestrial C cycling by 2100, analysis of variance (ANOVA) and wavelet clustering were applied to 70 projected simulation sets. In the end of simulation period, the changes from the year of 2000 in all three variables considerably varied from net negative to positive values. ANOVA revealed that the main sources of uncertainty are different among variables and depend on the projection period. We determined that in the global VegC, and SOC projections, GVMs dominate uncertainties (60 and 90 %, respectively) rather than climate driving scenarios, i.e., RCPs and GCMs. These results suggested that we don't have still enough resolution among each RCP scenario to evaluate climate change impacts on ecosystem conditions in global terrestrial C cycling. In addition, we found that the contributions of each uncertainty source were spatio-temporally heterogeneous and differed among the GVM variables. The dominant uncertainty source for changes in NPP and VegC varies along the climatic gradient. The contribution of GVM to the uncertainty decreases as the climate division gets cooler (from ca. 80 % in the equatorial division to 40 % in the snow climatic division). To evaluate the effects of climate change on ecosystems with practical resolution in RCP scenarios, GVMs require further improvement to reduce the uncertainties in global C cycling as much as, if not more than, GCMs. Our study suggests that the improvement of GVMs is a priority for the reduction of total uncertainties in projected C cycling for climate impact assessments.

ESDD
5, 1197–1219, 2014

1 Introduction

Terrestrial ecosystems play important roles in the C cycling of climate systems and in various ecosystem services (e.g., water supply, and wild habitats for biodiversity); however, their ecosystem functions are threatened by climate change (Scholze et al., 2006; Mooney et al., 2009). Previous model inter-comparison studies (e.g., VEMAP (Kittel et al., 1995), Potsdom DGVMs (Sitch et al., 2008), C4MIP (Friedlingstein et al., 2006), and CMIP5 Arora et al., 2013) have demonstrated a lack of coherence in future projections of terrestrial C cycling among global land models because of the differences in their representations of system processes. For climate change impact assessments, the cascade of uncertainty sources must be considered (Wilby and Dessai, 2010; Falloon et al., 2014). The concentrations of greenhouse gases, temperature, and precipitation are critical factors in determining the feedback of terrestrial ecosystems to atmospheric carbon dioxide (CO_2) (Seneviratne et al., 2006). These factors could become more important for terrestrial ecosystem C cycles under future higher CO_2 concentrations and climate change conditions (Gerten et al., 2005). The recent International Panel on Climate Change assessments (AR5) took anthropogenic CO_2 emission uncertainties into account in a Representative Concentration Pathway (RCP) scenario (Moss et al., 2010; Van Vuuren et al., 2011). Future changes in temperature and precipitation have large spatial and temporal uncertainties even at the same radiative forcing levels because of different structures and parameters of global climate models (GCM) (Knutti and Sedláček, 2013). These differences could affect the global C budget of terrestrial ecosystems. Global vegetation models (GVMs) (e.g., global dynamic vegetation model, components of earth system model) also have inherently large uncertainties because of differences in model structures and parameters (e.g. Friedlingstein et al., 2006; Sitch et al., 2008). Thus, for projected C cycling, various uncertainty sources exist across different phases.

For climate impact assessments and adaptations, different levels of uncertainty sources should be considered to manage climate change risks. Such information in

ESDD
5, 1197–1219, 2014

impacts assessments may benefit from experiences gained in the climate modeling community (and vice-versa) (Falloon et al., 2014). In addition, determining which uncertainty source is dominant in the projection is an import aspect in recognizing the limitations of ecosystem C cycling projection and climate impact assessment by means of GVM and GCM. However, to date, how each uncertainty source (CO_2 concentration, GCM, and GVM) matters in regions and periods affected by climate change still remain to be clarified in climate impacts research.

In this study, we examined C dynamics in six GVMs obtained from the Inter-sectoral Impact Model Intercomparison Project (ISI-MIP) (Warszawski et al., 2014). Four GVMs were used to investigate the possible responses of global natural terrestrial vegetation as part of ESMs in CMIP5 (Taylor et al., 2012). In ISI-MIP, these GVMs were simulated using five GCMs forced with four newly developed climate scenarios, i.e., RCP in CIMP5 experiments (Taylor et al., 2012). In this MIP, orthogonal experiment design on RCP, GCM, GVM was adopted. A total of 70 independent simulation sets were used in this study, which enabled us to evaluate the relative contributions to total uncertainty of the projection factors (emission scenarios, climate projections, and global vegetation models) in terrestrial C cycling. Our objective was to explore the comprehensive uncertainties in future global terrestrial C projections by inter-comparison of models.

2 Data and methods

2.1 Model and simulation protocol

We examined the global annual net primary production (NPP), vegetation biomass carbon stocks (VegC), and soil organic carbon (SOC) using six global vegetation models obtained from the ISI-MIP. The GVMs are Hybrid4 (Friend and White, 2000), JeDi (Pavlick et al., 2013), JULES (Clark et al., 2011), LPJmL (Sitch et al., 2003), SDGVM (Woodward et al., 1995), VISIT (Ito and Inatomi, 2012), which models simulated under multiple GCMs and RCPs in ISI-MIP. Hybrid4, Jedi, LPJmL, and JULES are dynamic

ESDD
5, 1197–1219, 2014

global vegetation models (DGVMs), and the other models use a fixed land cover map in this study. These models are simulated in 5 GCMs × 4 RCP scenarios. HadGEM2-ES (HadGEM), IPSL-CM5A-LR (IPSL), MIROC-ESM-CHEM (MIROC), GFDL-ESM2M (GFDL), and NorESM1-M (NorESM) are the GCMs from a CMIP5 experiment (Taylor et al., 2012) with bias correction for temperature and precipitation performed by Hempel et al. (2013). In this study, to focus on climate change impacts on terrestrial ecosystem C cycling, no anthropogenic land-use changes were considered in the simulation. The global climate variables (atmospheric CO_2 concentration, global mean temperature anomaly ΔT (°C), global precipitation anomaly ΔP (%)) in each RCP scenario for all GCMs are summarized in the Supplement.

2.2 Statistical analysis

We used three-way analysis of variance (ANOVA) for global ΔNPP, ΔVegC, and ΔSOC (changes from the year of 2000) at each year as factors for RCP, GCM, and GVM, and their interactions to decompose total variance in all ensembles into each factor (Yip et al., 2011). We calculated the Type II sum of square in ANOVA using R (R Core Team, 2012). In this study framework, overall uncertainty represented as variance ($\sigma^2_{\text{overall}}$) can be expressed as follows:

$$\sigma^2_{\text{overall}} = \sigma^2_{\text{RCP}} + \sigma^2_{\text{GCM}} + \sigma^2_{\text{GVM}} + \sigma^2_{\text{RCP}\times\text{GCM}} + \sigma^2_{\text{RCP}\times\text{GVM}} + \sigma^2_{\text{GCM}\times\text{GVM}} + \sigma^2_{\text{RCP}\times\text{GCM}\times\text{GVM}}$$

For grid-based assessment, also, we conducted ANOVA for ΔNPP, ΔVegC, and ΔSOC in each grid at two projection period (2055, 2099). For simplification, in grid based assessment, we have not considered the interaction terms (i.e., $\sigma^2_{\text{RCP}\times\text{GCM}}$, $\sigma^2_{\text{RCP}\times\text{GVM}}$, $\sigma^2_{\text{GCM}\times\text{GVM}}$, $\sigma^2_{\text{RCP}\times\text{GCM}\times\text{GVM}}$). In addition, from the grid-based maps, we compiled the dominant uncertainty source on the basis of the observation based present-day köppen-Geiger climatic divisions (Kottek et al., 2006). The five major climate types are equatorial (A), arid (B), warm temperature (C), snow (D), and polar climates (E).

ESDD
5, 1197–1219, 2014

We applied wavelet clustering (Rouyer et al., 2008) to the available ΔNPP, ΔVegC, and ΔSOC time series data set simulated under four RCP scenarios in all GCMs. Before applying this analysis, we standardized the time series data set to 0 at the year 2000, and applied wavelet transformation to each standardized data set to decompose the time series signal in both time and scale (Gouhier and Grinsted, 2012). With this information, after defining a metric to measure the pairwise distance among the extracted components, we built a dissimilarity matrix among the scenarios. Thus, we computed dissimilarity among multiple wavelet spectra of the time series data and clustered them using a hierarchical tree clustering method. This procedure enabled us to consider the variability of the time series in both time and frequency domains and to cope with aperiodic components, noise, and transient dynamics in the cluster analysis (Rouyer et al., 2008). To compare the dendrograms between each variable, we calculated the cophenetic correlation coefficient (Sokal and Rohlf, 1962).

3 Results

3.1 Global NPP, VegC, and SOC changes during 1970–2099

At the end of the simulation period, ΔNPP ranged from −7.0 to 54.3 Pg-C Year^{-1}, ΔVegC ranged from −27 to 543 Pg-C, and ΔSOC ranged from −195 to 471 Pg-C in the entire simulation set. The variance of ΔNPP increased with time and was the highest in RCP8.5. This was true for the other variables (ΔVegC and ΔSOC). NPP increased in RCP8.5, except in the Hybrid4 model. NPP in Hybrid4 forced with two GCMs (HadGEM and MIROC) showed negative values by 2099. Global VegC stocks increased in almost all RCPs and GVMs compared to global VegC in 2000. However, the global Veg stocks in LPJmL peaked at ca. 2050 and then declined toward 2100. In the projection period (2000–2099), the SOC stock in the five models (except for Hybrid4) increased in all RCPs compared to that in 2000.

ESDD
5, 1197–1219, 2014

3.2 The contribution of each uncertainty source to Global ΔNPP, ΔVegC, and ΔSOC

Figure 2 presents the fraction of uncertainty for each variable. For NPP, the GCM uncertainty dominated before the year 2020, and the RCP uncertainty increased and dominated after 2040. The GVM uncertainties were approximately 20 % in most of the simulation period. For VegC, the RCP uncertainty also increased gradually after 2020 and became approximately 40 % of the total variance by 2100. The GVM uncertainty dominated for most of the projection period; however, it decreased after 2040 by 40 % of the total variance. For SOC, the GVM uncertainty dominated throughout the projection period, and its average was 92 % of the total variance.

3.3 Global ΔNPP, ΔVegC, and ΔSOC

The clustering wavelet spectra identified three main groups for NPP, seven main groups for VegC, and four main groups for SOC (Fig. 3a–c). In the dendrogram of NPP (Fig. 3a), one cluster was aggregated mainly by the Hybrid4 model; however, all components (RCP, GCM, GVM) poorly differentiated aggregations in the other clusters. In the dendrogram of VegC, six clusters were mainly constituted by GVM, and another cluster comprised only one GCM (GFDL), including four GVMs. In the dendrogram of SOC, the main four clusters were clustered mostly on the basis of one or two GVMs rather than RCPs and GCMs. Considering each GVM model, in the JeDi cluster, the RCPs differentiated the clusters between RCP2.6 and RCP8.5 appropriately. However, there was no consistent trend for clustering by RCPs in other GVMs. The cophenetic correlation coefficients, i.e., the index of dendrogram similarity, were 0.01 ($p = 0.39$) between NPP and VegC, 0.04 ($p = 0.24$) between NPP and SOC, and 0.16 ($p < 0.01$) between VegC and SOC, which values indicate rather low similarities among the three dendrograms.

ESDD
5, 1197–1219, 2014

3.4 Regional maps

The strength of each uncertainty source to total variance showed geographically heterogenity in each variables (Fig. 4). For ΔNPP, GCM considerably contributed total variance in many parts of the world at 2055, however, at 2099, the variance mainly explained by GCM were observed in limited regions compared to those at 2099. RCP dominant uncertainty source regions were observed in part of tropics (South East Asia) to cool temperate regions (North America) in 2099 for ΔNPP. For ΔVegC, GCM are more dominant contributions to each grid total variance in almost regions at both periods. For ΔSOC, GVM was dominant uncertainty source to each grid total variance in almost regions in both periods. GCM was observed as the dominant uncertainty source in some regions such as South-West US, Sahara regions for ΔSOC.

In terms of climatic divisions, the dominant uncertainty source clearly showed different patterns in ΔNPP and ΔVegC along with the equatorial climate (A) to the snow climate (D) (Fig. 5). The contribution of GVM to ΔNPP variance decreases as the climate gets cooler in NPP (Fig. 5a). In the each major climatic division, the seasonally drier divisions (m, s, w) tended to showed a higher contribution of GCM, compared to the division with fully humid season (f). Similarly, in the arid climates (BW and BS), the contribution of GCM to the uncertainties in all variables was relatively higher contributions to the uncertainties in all variables (Fig. 5a–c). Unlike global ΔNPP and global ΔVegC, GVM was dominant in tropic climates (Af – Aw), while RCP are not dominant in these regions, even in 2100. In Cf, Ds, Dw, and ET, RCP was the first and second dominant uncertainty source (from 30 to 50 % area) in each climatic division. For ΔSOC, GVM were dominant in a broad area of all climate divisions as seen for shown in global ΔSOC. In addition, there were negligible areas where RCP dominate the uncertainty in ΔSOC for all climatic divisions.

ESDD
5, 1197–1219, 2014

4 Discussions

In the historical period (1970–2000), models simulated historical NPP, VegC, and SOC trends in the same way among GCMs. However, at the end of projection period, the differences were markedly broad for all variables (Fig. 1). In particular, NPP and SOC varied from a net sink to a net source in the highest baseline emission scenario (RCP8.5). In higher emission scenarios, the total uncertainties for all variables increased to a greater extent. The total uncertainties for each variable in this study were comparable or greater than those for the projected C cycling in a previous inter-comparison of model (Sitch et al., 2008; Todd-Brown et al., 2013) even with a smaller number of GVMs.

Compared to previous model inter-comparison studies regarding terrestrial C cycling, the ISI-MIP study has an important simulation protocol advantage, i.e., it is a partial factorial experiment with three independent treatments of CO_2 emission scenario (RCP), GCM, and GVM. Therefore, uncertainty can be decomposed to the sum of inter-class variance (σ^2_{RCP}, σ^2_{GCM}, σ^2_{GVM}, and the interactions) and within-class variance (σ^2_{resid}). The ANOVA results revealed quite different contributions to the total uncertainties for each source, and it varied with projection period (Fig. 2). While GCMs are dominant sources of uncertainty for NPP early in the projection period (2000–2040), RCP dominates later in the projection period (2050–2100) (Fig. 2). This trend of increasing RCP importance is similar to VegC (Fig. 2). This may be attributed to the enlargement of CO_2 concentration difference among RCPs in this period. The interaction terms as a uncertainty source were significant ($p < 0.05$ level, not described) and contributed considerably to total uncertainties (up to 20 %) in NPP, indicating that different sensitivities to the CO_2 fertilization effect on vegetation processes among the GVMs (Friend et al., 2014) also contributed to projection uncertainties. Regarding the CO_2 fertilization effect, for NPP and VegC, the cluster analysis suggested uniqueness in the Hybrid4 model projection (Fig. 3a and b). This is partially due to Hybrid4 having strong stomatal responses to elevated vapor pressure deficits, and thus simulated

ESDD
5, 1197–1219, 2014

negative NPP between 2080–2100 even in higher CO_2 condition (Friend et al., 2014). Furthermore, only Hybrid4 has a fully coupled N cycle in this study, therefore, as well as CO_2 fertilization effect, the implementation of the N cycle in more models is required for more plausible effects of CO_2 fertilization in terrestrial C projection (Thornton et al., 2009).

On the other hand, the uncertainties in SOC changes driven by GVM are substantially large and were dominant in the entire simulation period (Fig. 2), which may suggest that SOC processes are not well constrained by the observation data or between models. RCPs and GCMs differentiated clusters poorly for the time series data of global SOC stocks (Fig. 3c), suggesting that the uncertainties derived from the GVMs overwhelmed those derived from the climate scenarios. In addition, our analysis showed that the cluster dendrogram for VegC (Fig. 3b) did not correlate strongly with that for SOC (R = 0.16 in cophenetic correlation), i.e., the SOC processes contributed considerably to GVM-driven clustering in the dendrogram for SOC. Another ISI-MIP study has shown that the sensitivity of global SOC decomposition to increasing global mean temperature varied significantly among GVMs (Nishina et al., 2014). Temperature sensitivities of SOC may be one of the key factors for reducing terrestrial C projection uncertainty.

In light of geographic distribution, we found the contributions of each uncertainty source to each grid variance were spatially heterogenous (Fig. 5), although the total contributions of each uncertainty source in grid based assessment (Fig. 4) are roughly agreed with Fig. 2 in each period (2050, 2099). These heterogeneities could be coordinated with the climatic divisions (Fig. 5). For example, in ΔSOC, GVMs is also main contributor in almost regions in both periods (2050 and 2099). However, the grid based assessment revealed geographically distinct regions in each uncertainty source. Although GCM was not large contributor in global SOC dynamics (Figs. 4 and 5), GCM largely contributed the uncertainty in arid (BW) to semi-arid (BS) regions (e.g., Sub Sahara, South-West US, South America (Pampa), Central Asia, Australia) in all variables. In CMIP5 study, Sillmann et al. (2013) reported that changes in precipitation patterns

ESDD
5, 1197–1219, 2014

in their regions showed the low degree of coincidence among GCMs. These results suggest that the projection of precipitation patterns among GCMs are critically important to evaluate climate change impact on ecosystem conditions and their C stocks in these regions (figure as in supplemental file). Although the carbon stocks and changes in their regions are not large, it it important to predict local climate condition uncertainties for local climate prediction of ecosystem changes under climate change. In NPP and VegC at 2099, GVM is dominant source in semitropical-to-tropical climate zones (especially in south-east Asia, Latin America, Central Africa), whereas GVM is not dominant in global ΔNPP in this period. This implicated that modification of tropical rainforest C cycling is critical for to reduce uncertainties in global NPP. In broad terms, the contribution of GVM as an uncertainty source in ΔNPP become less in the cooler climatic regions (C–D); however, the contributions of GVM to ΔVegC were larger in the cooler climatic regions (Fig. 5). This inconsistency can be explained by the large differences in vegetation turnover rate in the northern ecosystems among GVMs because of the different representations of vegetation dynamic processes (i.e., forest fire, N cycle, senescence, and so on) (Friend et al., 2014). These results highlight that model improvement on the basis of plant functional type (corresponding to the climate divisions) could be important to effectively reduce uncertainty in climate impact assessments.

Our results do not mean that GCMs are not important to the uncertainties of VegC and SOC projection from the point of global C stocks. For example, under RCP8.5, the Hybrid4 model simulated that VegC diverged considerably among GCMs by 2100 (from 162 to 547 Pg-C). In addition, one of the GCMs (GFDL) identified a small cluster across four GVMs for VegC (Fig. 3b). Moreover, in Ahlström et al. (2012), one DGVM forced with 10 different GCMs showed a difference of approximately 500 Pg-C among the projections of global terrestrial C stock (VegC & SOC) changes by 2100. Also, we should pay attention to the numbers of GCMs and impact models in our study would affect the results. Hence, our results indicate a smaller contribution by GCM to total uncertainties than a lack of inter-global vegetation model constraints due to insufficient validations in SOC and VegC processes by global observations. In the case

ESDD
5, 1197–1219, 2014

of RCP2.6, the model projections were comparable for ΔNPP; however, ΔVegC and ΔSOC differed significantly. This implies that internal ecosystem processes such as photosynthate partitioning and mortality were poorly constrained in the GVMs. Also, their process uncertainties considerably affect SOC dynamics as a C source via litter inputs. More observation-based model inter-comparison (e.g., MsTMIP, Huntzinger et al., 2012) by each component is required for GVMs to reduce overall uncertainty. For SOC dynamics, the empirical estimations using observation-based heterotrophic respiration (Bond-Lamberty and Thomson, 2010; Hashimoto, 2012) are available for validation of SOC decomposition processes. In addition to each model modification, in future, multiple land-use scenarios should also be considered in projections to comprehend additional potential uncertainties ($\sigma^2_{\text{land.use}}$) in the global terrestrial C budget. Also, the use of bias-corrected GCM forcing data will likely affect the C dynamics as well as the projections in hydrological models (Haddeland et al., 2011; Ehret et al., 2012), however, there were still lack of validation in the effect of various bias correction methods on C cycling projection and their relative uncertainty.

5 Conclusions

In conclusion, by combining multiple GVMs, GCMs, and RCP scenarios, we found the different contributions of each factor to total uncertainty, which is highly dependent on the variables (NPP, VegC, and SOC), projection periods, and regions. The contribution of each source of uncertainty in these variables showed different patterns against the hydrological variable simulated by global hydrological models from another ISI-MIP study (Wada et al., 2013). In particular, for global SOC projection, uncertainty driven by GVM was greater than that of climate scenarios, i.e., RCPs and GCMs. The uncertainties associated with SOC projections are significantly high, and the global SOC stocks by 2099 shift from net CO_2 sources to net sinks (from −195 to 471 Pg-C). The CO_2 emission scenario (RCP) as an uncertainty source is important for the late projection period for both NPP and VegC. Moreover, CO_2 fertilization sensitivity of vegetation

ESDD
5, 1197–1219, 2014

processes is important quantitatively for future C projection uncertainty. To evaluate climate change impacts on ecosystem with practical resolution to RCP scenarios, GVMs require further improvement to reduce global C cycling uncertainties as much as, if not more than, GCMs.

The Supplement related to this article is available online at doi:10.5194/esdd-5-1197-2014-supplement.

Acknowledgements. We wish to thank the ISI-MIP coordination team of the Potsdam Institute for Climate Impact Research. We also acknowledge the World Climate Research Programme's Working Group on Coupled Modelling, which is responsible for CMIP, and we thank the climate modeling groups for producing and making their model output available. The ISI-MIP Fast Track project was funded by the German Federal Ministry of Education and Research (BMBF), with project funding reference number 01LS1201A. K. Nishina, A. Ito, E. Kato, and T. Yokohata were supported by the Environment Research and Technology Development Fund (S-10) of the Ministry of the Environment, Japan.

References

Ahlström, A., Schurgers, G., Arneth, A., and Smith, B.: Robustness and uncertainty in terrestrial ecosystem carbon response to CMIP5 climate change projections, Environ. Res. Lett., 7, 044008, doi:10.1088/1748-9326/7/4/044008, 2012. 1208

Arora, V. K., Boer, G. J., Friedlingstein, P., Eby, M., Jones, C. D., Christian, J. R., Bonan, G., Bopp, L., Brovkin, V., Cadule, P., Hajima, T., Ilyina, T., Lindsay, K., Tjiputra, J. F., and Wu, T: Carbon-concentration and carbon-climate feedbacks in CMIP5 Earth system models, J. Climate, 26, 5289–5314, 2013. 1200

Bond-Lamberty, B. and Thomson, A.: Temperature-associated increases in the global soil respiration record, Nature, 464, 579–582, 2010. 1209

Clark, D. B., Mercado, L. M., Sitch, S., Jones, C. D., Gedney, N., Best, M. J., Pryor, M., Rooney, G. G., Essery, R. L. H., Blyth, E., Boucher, O., Harding, R. J., Huntingford, C., and

ESDD
5, 1197–1219, 2014

Cox, P. M.: The Joint UK Land Environment Simulator (JULES), model description – Part 2: Carbon fluxes and vegetation dynamics, Geosci. Model Dev., 4, 701–722, doi:10.5194/gmd-4-701-2011, 2011. 1201

Ehret, U., Zehe, E., Wulfmeyer, V., Warrach-Sagi, K., and Liebert, J.: HESS Opinions "Should we apply bias correction to global and regional climate model data?", Hydrol. Earth Syst. Sci., 16, 3391–3404, doi:10.5194/hess-16-3391-2012, 2012. 1209

Falloon, P., Challinor, A., Dessai, S., Hoang, L., Johnson, J., and Koehler, A.-K.: Ensembles and uncertainty in climate change impacts, Front. Environ. Sci., 2, doi:10.3389/fenvs.2014.00033, 2014. 1200, 1201

Friedlingstein, P., Cox, P., Betts, R., Bopp, L., Von Bloh, W., Brovkin, V., Cadule, P., Doney, S., Eby, M., Fung, I., Govindasamy, B., John, J., Jones, C., Joos, F., Kato, T., Kawamiya, M., Knorr, W., Lindsay, K., Matthews, H. D., Raddatz, T., Rayner, P., Reick, C., Roeckner, E., Schnitzler, K.-G., Schnur, R., Strassmann, K., Thompson, S., Weaver, A. J., Yoshikawa, C., and Zeng, N.: Climate-carbon cycle feedback analysis: results from the C4MIP model intercomparison, J. Climate, 19, 3337–3353, 2006. 1200

Friend, A. D. and White, A.: Evaluation and analysis of a dynamic terrestrial ecosystem model under preindustrial conditions at the global scale, Global Biogeochem. Cy., 14, 1173–1190, 2000. 1201

Friend, A. D., Lucht, W., Rademacher, T. T., Keribin, R., Betts, R., Cadule, P., Ciais, P., Clark, D. B., Dankers, R., Falloon, P. D., Ito, A., Kahana, R., Kleidon, A., Lomas, M. R., Nishina, K., Ostberg, S., Pavlick, R., Peylin, P., Schaphoff, S., Vuichard, N., Warszawski, L., Wiltshire, A., and Woodward, F. I.: Carbon residence time dominates uncertainty in terrestrial vegetation responses to future climate and atmospheric CO_2, P. Natl. Acad. Sci. USA, 111, 3280–3285, 2014. 1206, 1207, 1208

Gerten, D., Lucht, W., Schaphoff, S., Cramer, W., Hickler, T., and Wagner, W.: Hydrologic resilience of the terrestrial biosphere, Geophys. Res. Lett., 32, L21408, doi:10.1029/2005GL024247, 2005. 1200

Gouhier, T. C. and Grinsted, A.: Biwavelet: conduct univariate and bivariate wavelet analyses, available at: http://CRAN.R-project.org/package=biwavelet (last access: August 2014), R package version 0.12, 2012. 1203

Haddeland, I., Clark, D. B., Franssen, W., Ludwig, F., Voß, F., Arnell, N. W., Bertrand, N., Best, M., Folwell, S., Gerten, D., Gomes, S., Gosling, S. N., Hagemann, S., Hanasaki, N., Harding, R., Heinke, J., Kabat, P., Koirala, S., Oki, T., Polcher, J., Stacke, T., Viterbo, P., Weedon, G.

ESDD
5, 1197–1219, 2014

P., and Yeh, P.: Multimodel estimate of the global terrestrial water balance: Setup and first results, J. Hydrometeorol., 12, 869–884, 2011. 1209
Hashimoto, S.: A new estimation of global soil greenhouse gas fluxes using a simple data-oriented model, PloS one, 7, e41962, doi:10.1371/journal.pone.0041962, 2012. 1209
Hempel, S., Frieler, K., Warszawski, L., Schewe, J., and Piontek, F.: A trend-preserving bias correction – the ISI-MIP approach, Earth Syst. Dynam., 4, 219–236, doi:10.5194/esd-4-219-2013, 2013. 1202
Huntzinger, D., Post, W. M., Wei, Y., Michalak, A., West, T. O., Jacobson, A., Baker, I., Chen, J. M., Davis, K., Hayes, D., Hoffman, F. M., Jain, A. K., Liu, S., McGuire, A. D., Neilson, R. P., Potter, C., Poulter, B., Price, D., Raczka, B. M., Tian, H. Q., Thornton, P., Tomelleri, E., Viovy, N., Xiao, J., Yuan, W., Zeng, N., Zhao, M., and Cook, R.: North American Carbon Program (NACP) regional interim synthesis: terrestrial biospheric model intercomparison, Ecol. Model., 232, 144–157, 2012. 1209
Ito, A. and Inatomi, M.: Water-use efficiency of the terrestrial biosphere: a model analysis focusing on interactions between the global carbon and water cycles, J. Hydrometeorol., 13, 681–694, 2012. 1201
Kittel, T., Rosenbloom, N., Painter, T., and Schimel, D.: The VEMAP integrated database for modelling United States ecosystem/vegetation sensitivity to climate change, J. Biogeogr., 22, 857–862, 1995. 1200
Knutti, R. and Sedláček, J.: Robustness and uncertainties in the new CMIP5 climate model projections, Nat. Clim. Change, 3, 369–373, doi:10.1038/nclimate1716, 2013. 1200
Kottek, M., Grieser, J., Beck, C., Rudolf, B., and Rubel, F.: World map of the Köppen-Geiger climate classification updated, Meteorol. Z., 15, 259–263, 2006. 1202
Mooney, H., Larigauderie, A., Cesario, M., Elmquist, T., Hoegh-Guldberg, O., Lavorel, S., Mace, G. M., Palmer, M., Scholes, R., and Yahara, T.: Biodiversity, climate change, and ecosystem services, Curr. Opin. Environ. Sustain., 1, 46–54, 2009. 1200
Moss, R. H., Edmonds, J. A., Hibbard, K. A., Manning, M. R., Rose, S. K., van Vuuren, D. P., Carter, T. R., Emori, S., Kainuma, M., Kram, T., Meehl, G. A., Mitchell, J. F. B., Nakicenovic, N., Riahi, K., Smith, S. J., Stouffer, R. J., Thomson, A. M., Weyant, J. P., and Wilbanks, T. J.: The next generation of scenarios for climate change research and assessment, Nature, 463, 747–756, 2010. 1200
Nishina, K., Ito, A., Beerling, D. J., Cadule, P., Ciais, P., Clark, D. B., Falloon, P., Friend, A. D., Kahana, R., Kato, E., Keribin, R., Lucht, W., Lomas, M., Rademacher, T. T., Pavlick, R.,

ESDD
5, 1197–1219, 2014

Schaphoff, S., Vuichard, N., Warszawaski, L., and Yokohata, T.: Quantifying uncertainties in soil carbon responses to changes in global mean temperature and precipitation, Earth Syst. Dynam., 5, 197–209, doi:10.5194/esd-5-197-2014, 2014. 1207

Pavlick, R., Drewry, D. T., Bohn, K., Reu, B., and Kleidon, A.: The Jena Diversity-Dynamic Global Vegetation Model (JeDi-DGVM): a diverse approach to representing terrestrial biogeography and biogeochemistry based on plant functional trade-offs, Biogeosciences, 10, 4137–4177, doi:10.5194/bg-10-4137-2013, 2013. 1201

R Core Team: R: A Language and Environment for Statistical Computing, R Foundation for Statistical Computing, Vienna, Austria, available at: http://www.R-project.org/ (last access: August 2014), ISBN 3-900051-07-0, 2012. 1202

Rouyer, T., Fromentin, J., Ménard, F., Cazelles, B., Briand, K., Pianet, R., Planque, B., and Stenseth, N.: Complex interplays among population dynamics, environmental forcing, and exploitation in fisheries, Proc. Natl. Acad. Sci. USA, 105, 5420–5425, 2008. 1203

Scholze, M., Knorr, W., Arnell, N. W., and Prentice, I. C.: A climate-change risk analysis for world ecosystems, Proc. Natl. Acad. Sci. USA, 103, 13116–13120, 2006. 1200

Seneviratne, S., Lüthi, D., Litschi, M., and Schär, C.: Land-atmosphere coupling and climate change in Europe, Nature, 443, 205–209, 2006. 1200

Sillmann, J., Kharin, V., Zwiers, F., Zhang, X., and Bronaugh, D.: Climate extremes indices in the CMIP5 multimodel ensemble: Part 2. Future climate projections, J. Geophys. Res.-Atmos., 118, 2473–2493, 2013. 1207

Sitch, S., Smith, B., Prentice, I., Arneth, A., Bondeau, A., Cramer, W., Kaplan, J., Levis, S., Lucht, W., Sykes, M., Thonicke, K., and Venevsky, S.: Evaluation of ecosystem dynamics, plant geography and terrestrial carbon cycling in the LPJ dynamic global vegetation model, Glob. Change Biol., 9, 161–185, 2003. 1201

Sitch, S., Huntingford, C., Gedney, N., Levy, P., Lomas, M., Piao, S., Betts, R., Ciais, P., Cox, P., Friedlingstein, P., Jones, C. D., Prentice, I. C., and Woodward, F. I.: Evaluation of the terrestrial carbon cycle, future plant geography and climate-carbon cycle feedbacks using five Dynamic Global Vegetation Models (DGVMs), Glob. Change Biol., 14, 2015–2039, 2008. 1200, 1206

Sokal, R. R. and Rohlf, F. J.: The comparison of dendrograms by objective methods, Taxon, 11, 33–40, 1962. 1203

Taylor, K. E., Stouffer, R. J., and Meehl, G. A.: An overview of CMIP5 and the experiment design, B. Am. Meteorol. Soc., 93, 485–498, 2012. 1201, 1202

ESDD
5, 1197–1219, 2014

Thornton, P. E., Doney, S. C., Lindsay, K., Moore, J. K., Mahowald, N., Randerson, J. T., Fung, I., Lamarque, J.-F., Feddema, J. J., and Lee, Y.-H.: Carbon-nitrogen interactions regulate climate-carbon cycle feedbacks: results from an atmosphere-ocean general circulation model, Biogeosciences, 6, 2099–2120, doi:10.5194/bg-6-2099-2009, 2009. 1207

Todd-Brown, K. E. O., Randerson, J. T., Post, W. M., Hoffman, F. M., Tarnocai, C., Schuur, E. A. G., and Allison, S. D.: Causes of variation in soil carbon simulations from CMIP5 Earth system models and comparison with observations, Biogeosciences, 10, 1717–1736, doi:10.5194/bg-10-1717-2013, 2013. 1206

Van Vuuren, D. P., Edmonds, J., Kainuma, M., Riahi, K., Thomson, A., Hibbard, K., Hurtt, G. C., Kram, T., Krey, V., Lamarque, J.-F., Masui, T., Meinshausen, M., Nakicenovic, N., Smith, S. J., and Rose, S. K.: The representative concentration pathways: an overview, Clim. Change, 109, 5–31, 2011. 1200

Wada, Y., Wisser, D., Eisner, S., Flörke, M., Gerten, D., Haddeland, I., Hanasaki, N., Masaki, Y., Portmann, F. T., Stacke, T., Tessler, Z., and Schewe, J.: Multimodel projections and uncertainties of irrigation water demand under climate change, Geophys. Res. Lett., 40, 4626–4632, doi:10.1002/grl.50686, 2013. 1209

Warszawski, L., Frieler, K., Huber, V., Piontek, F., Serdeczny, O., and Schewe, J.: The Inter-Sectoral Impact Model Intercomparison Project (ISI–MIP): project framework, Proc. Natl. Acad. Sci. USA, 111, 3228–3232, 2014. 1201

Wilby, R. L. and Dessai, S.: Robust adaptation to climate change, Weather, 65, 180–185, 2010. 1200

Woodward, F., Smith, T., and Emanuel, W.: A global land primary productivity and phytogeography model, Global Biogeochem. Cy., 9, 471–490, 1995. 1201

Yip, S., Ferro, C. A., Stephenson, D. B., and Hawkins, E.: A simple, coherent framework for partitioning uncertainty in climate predictions, J. Climate, 24, 4634–4643, 2011. 1202

ESDD
5, 1197–1219, 2014

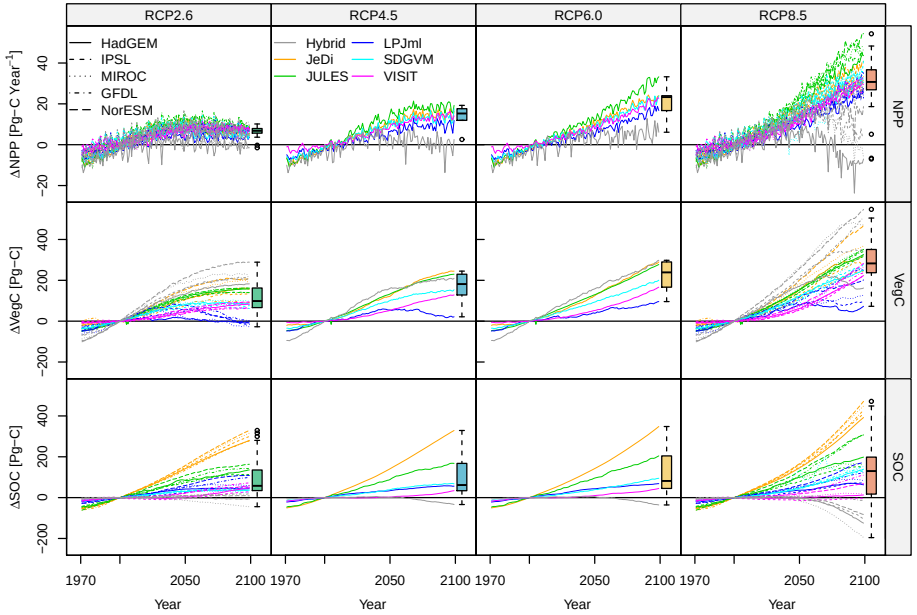

Figure 1. Global annual NPP, VegC stock, and SOC stock changes. The boxplot summarizes the values at the end of simulation period. Open circles represent outliers if the largest (or smallest) value is greater (or less) than 1.5 times the box length from the 75 % percentile (or 25 % percentile).

ESDD
5, 1197–1219, 2014

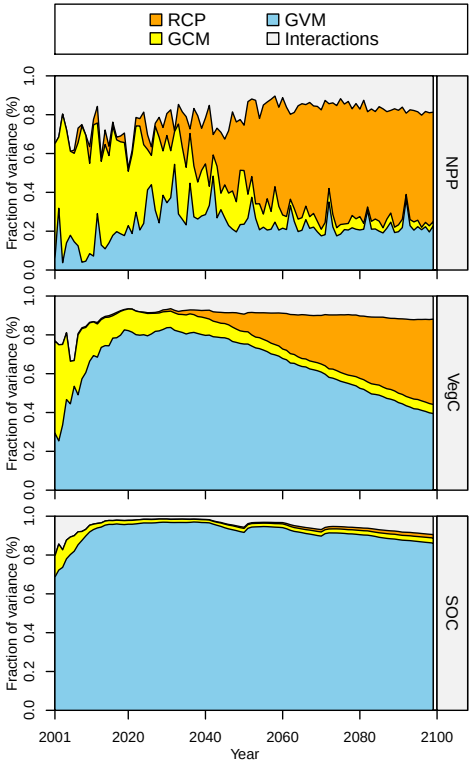

Figure 2. Fraction of variance derived from the emission scenario (RCPs), GCMs, and GVMs for annual NPP, VegC, and SOC changes. The variances were estimated by three-way ANOVA. The fraction in interactions includes the sum of variations of interaction terms (RCP × GCM, RCP × GVM, and GCM × GVM).

ESDD
5, 1197–1219, 2014

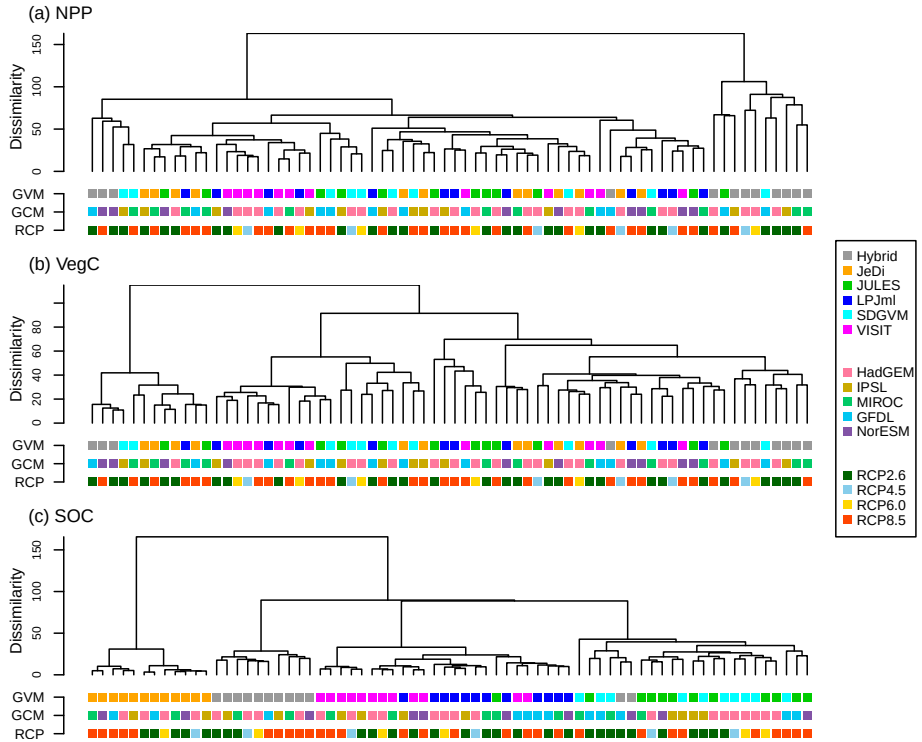

Figure 3. Cluster tree of wavelet spectra for the NPP **(a)**, VegC **(b)**, and SOC **(c)** for 5 GCMs × 4 RCPs from 1971–2099.

ESDD
5, 1197–1219, 2014

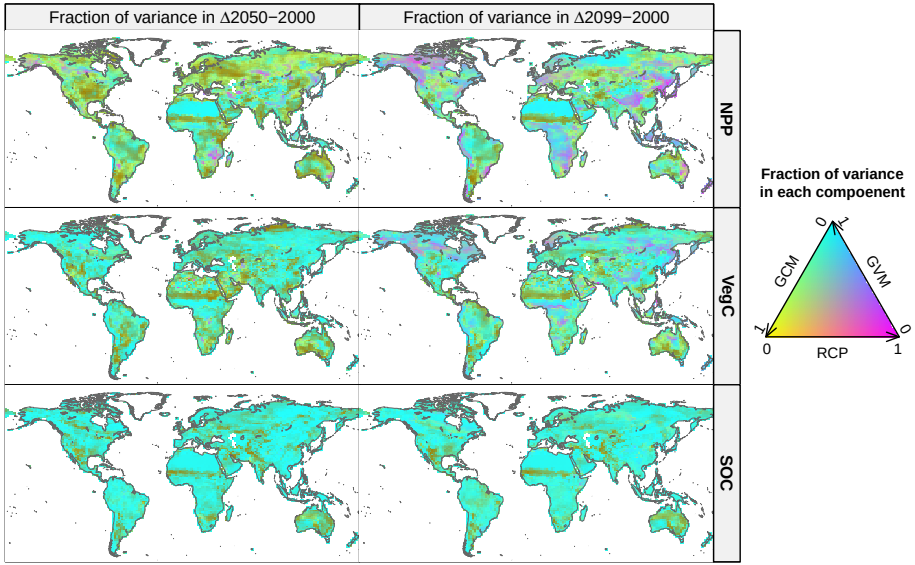

Figure 4. Geographic distribution of fraction of variance derived from the emission scenario (RCPs), GCMs, and GVMs for annual NPP, VegC, and SOC changes from 2000 to 2050 and 2099 in each grid cell. The variances were estimated by one-way ANOVA.

ESDD
5, 1197–1219, 2014

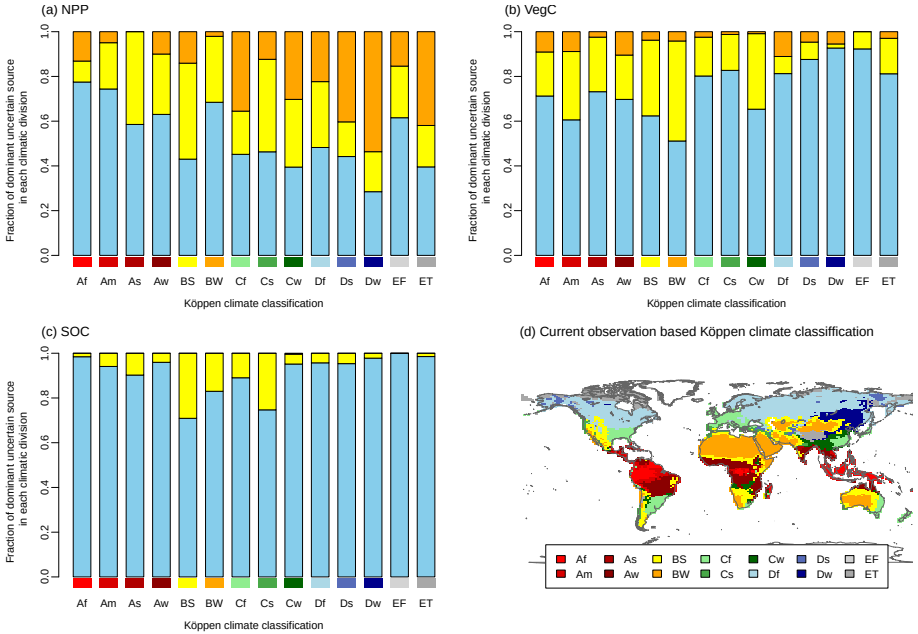

Figure 5. The fraction of dominant uncertainty source in each Köppen climatic divisions in ΔNPP **(a)**, ΔVegC **(b)**, ΔSOC **(c)** in 2099, and Köppen climate classification map for the period 1951 to 2000 in CRU **(d)**. In **(a–c)**, color indicate each uncertainty source as in Fig. 2 (i.e., Orange indicates RCP. Yellow indicates GCM. Blue indicates GVM).

ESDD
5, 1197–1219, 2014